SYNTHETIC BIOLOGY

High-fidelity human chromosome transfer and elimination

Gianluca Petris[1,2]†‡, Simona Grazioli[1]†, Linda van Bijsterveldt[1]†, Pierre Murat[1]§, Kim C. Liu[1], Jakob Birnbaum[1]¶, Julian E. Sale[1,2]*, Jason W. Chin[1,2]*

The synthesis of human genomes and other gigabase-scale genomes will require new strategies. Here, we realized key steps in our pipeline for building synthetic human chromosomes. We established: (i) the facile transfer of human chromosomes from human cells to mouse embryonic stem cells (assembly cells), where they are haploid, are nonessential, and may be operated on; (ii) the transfer of these human chromosomes from monochromosomal hybrids back into human cells to generate defined, synthetic aneuploidies; and (iii) the elimination of the corresponding endogenous human chromosomes to regenerate diploid cells containing a transferred chromosome. All steps were performed in nontransformed cells without chromothripsis and generated minimal structural variants, insertions, deletions, or single-nucleotide variants.

Human genome synthesis will facilitate an understanding of the causal relationships and rules underpinning the sequence and architecture of natural genomes, enable the construction of extinct hominid genotypes, accelerate bioproduction, and improve cell-based therapies.

Human chromosomes are too large to be assembled in the microbial hosts that have been used for *Mycoplasma genitalium* and *Escherichia coli* genome syntheses (*1*, *2*) and for *Saccharomyces cerevisiae* chromosome syntheses (*3*, *4*), and the repetitive nature of human DNA makes its large-scale maintenance and manipulation difficult or impossible in recombinogenic organisms such as *S. cerevisiae*. Targeted manipulation of a single copy of a human chromosome in a human cell with a diploid genome is also challenging. A major current goal is therefore to develop approaches to address the challenges of human genome synthesis.

We set out to establish a strategy for building human chromosomes and genomes (Fig. 1 and fig. S1). This strategy generates a single copy of a human chromosome in assembly cells, mouse embryonic stem cells (mESCs) (see the supplementary text), so that its sequence can be specifically targeted. The use of assembly cells reduces the risk of recombination between the engineered human chromosome and the rest of the genome and eliminates the risk of interallelic recombination for the engineered human chromosome. Because human chromosomes are nonessential in assembly cells, additional manipulations (e.g., deletions of essential and haploinsufficient genes) will become possible. Moreover, off-target mutations in the host genome (as a by-product of targeted manipulation of the human chromosome) will not be carried through to the final human cell.

Our approach requires the transfer of intact human chromosomes from human cells into mESCs to generate monochromosomal hybrids, the transfer of chromosomes from monochromosomal hybrids into human cells to generate defined synthetic human aneuploidies, and the targeted elimination of an endogenous chromosome to regenerate human cells with a normal karyotype and a transferred chromosome. In the present work, we addressed the challenges associated with each of these steps (see the supplementary text).

[1]Medical Research Council Laboratory of Molecular Biology, Cambridge, UK. [2]Wellcome Sanger Institute, Wellcome Trust Genome Campus, Hinxton, UK. ***Corresponding author. Email: jes@mrc-lmb.cam.ac.uk (J.E.S.); chin@mrc-lmb.cam.ac.uk (J.W.C.)** †These authors contributed equally to this work. ‡Present address: Università degli Studi di Udine, Udine, Italy, and Fondazione Italiana Fegato, Basovizza, Trieste, Italy. §Present address: Wellcome Sanger Institute, Wellcome Trust Genome Campus, Hinxton, UK. ¶Present address: AstraZeneca, Hamburg, Germany.

Labeling chromosomes in RPE1 donor cells

We selected the nontransformed and immortalized human RPE1 cell line (*5*), which has a stable, near-diploid karyotype (fig. S2, A and B) (*6*), as the donor for our chromosome transfer experiments.

To facilitate the subsequent identification and isolation of chromosome transfer events in the recipient mESCs, we marked all chromosomes in the RPE1 donor using a *PiggyBac* cassette containing superfolder green fluorescent protein (sfGFP) and a neomycin resistance gene conferring resistance to G418 (sfGFP-NEO) (*7*, *8*) (fig. S3A). We confirmed the labeling of all 23 chromosomes (fig. S3B). The integration sites were distributed evenly across the genome and showed a correlation between the number of integrations in each chromosome and its length (fig. S3, C and D).

Transfer of human chromosomes from human cells to mESCs

We arrested the sfGFP-NEO RPE1 donor cells in M phase with colcemid for 6 to 9 hours (see the materials and methods) (fig. S2C) and incubated mitotic cells with the actin polymerization inhibitor latrunculin B (*9*). Condensed chromosomes were released from cells into protective polyamine buffer (*10*) (see the materials and methods), and the resulting chromosome suspension was transfected into mESCs with polyethylenimine (PEI) (Fig. 2A), achieving a transfection efficiency of ~10^{-6}.

After 13 independent chromosome transfection experiments, we obtained a library of 49 G418-resistant mESC clones. Overall, G418-resistant mESC clones spanned 13 different human chromosomes (4, 5, 6, 8, 9, 10, 12, 13, 14, 19, 20, 21, and 22) and harbored human chromosomes [intact, fragmented, or displaying internal copy number variations (CNVs)] (figs. S4, A to D, and S5; table S1; and supplementary text), as judged by low-coverage whole-genome sequencing (WGS). Thirteen mESC clones likely had an intact human chromosome (4, 6, 10, 13, 20, and 21) (figs. S4, A and B, and S5 and table S1). The number of distinct human chromosomes (or chromosome fragments) present in the library of monochromosomal hybrids showed minimal deviation from the values expected for the unbiased transfer of chromosomes (or their fragments) (fig. S4, E to G). We performed chromosome stability analyses based on sfGFP maintenance (fig. S6) and showed that fluorescence in situ hybridization (FISH) (fig. S7) was consistent with low-coverage WGS, confirming the presence of clones containing a single intact human chromosome (see the supplementary text).

Next, we more deeply characterized three mESC clones, mESC Hchr4 (CL3), mESC Hchr21 (CT2-1), and mESC Hchr20 (CB20F), for which our initial analyses, along with G-banding analysis and flow karyotyping (see the supplementary text), were consistent with the presence of a single intact human chromosome (Fig. 2, B and C, and figs. S8A and S9). These clones cover the three types of human chromosomes, submetacentric (chromosome 4; 193.5 Mb), metacentric (chromosome 20; 66.2 Mb), and acrocentric (chromosome 21; 45.1 Mb). We performed high-coverage (20 to 30×) Illumina WGS, long-read Oxford nanopore sequencing (Oxford Nanopore Technologies, ONT), PacBio sequencing, and Bionano optical genome mapping (OGM) on these three clones (Fig. 2, D to G; figs. S8, B and C, and S10 and S11; and supplementary text). From an analysis of the resulting data, we concluded that there was a single copy of each human chromosome in the assembly cells (Fig. 2, D and E, and fig. S8B) and that occurrences of CNVs, structural variants (SVs), insertions and deletions (INDELs), and single-nucleotide variants (SNVs) in intact human chromosomes in mESCs were low and deviated minimally from their frequencies in parental, human RPE1 cells (Fig. 2, H and I, and fig. S8D).

Additionally, we characterized three further monochromosomal hybrid clones, mESC Hchr6 (CB20-GO), mESC Hchr10 (CB15C), and

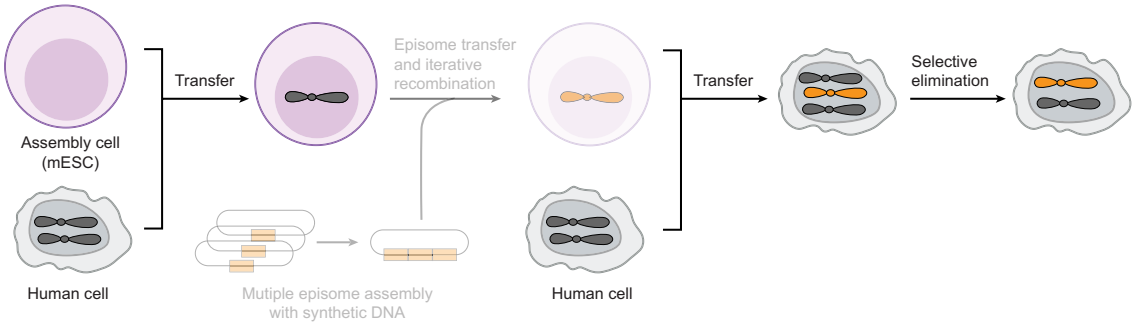

Fig. 1. Overview of our strategy for the generation of human cells bearing synthetic human chromosomes. In the present work, we focused on the transfer of human chromosomes from human cells to assembly cells, the transfer of human chromosomes from assembly cells to human cells to generate defined aneuploidies, and the elimination of targeted endogenous chromosomes to generate a diploid cell bearing the transferred chromosome. These operations are shown in the solid part of the image. The operations necessary to convert the human chromosome into a synthetic chromosome are shown as translucent illustrations and captions. These steps include the assembly of episomes bearing synthetic human DNA and the transfer and recombination of this DNA into the human chromosome. Progress on these steps is discussed in the supplementary text and in the legend to fig. S1.

mESC Hchr13 (CT-3). Our analyses (fig. S12, A to C; table S1; and supplementary text) indicated that we had successfully transfected these three additional human chromosomes into mESCs without detectable gross rearrangements. The six transferred chromosomes harbored a density of genes and genomic features [e.g., GC content, long (LINE) and short (SINE) Interspersed nuclear element density, and repetitive elements] that were at comparable levels to their median levels across the human genome (fig. S12D), further supporting the view that the workflow is generalizable to other human chromosomes.

We estimated telomere length in chromosome arms using OGM by measuring the distance from the last marker detected to the end of individual DNA molecules (*11*) (see the materials and methods). In RPE1 cells, the telomere molecule lengths for Hchr4 (4p and 4q) and Hchr21 (21q) ranged from 5 to 10 kb (Fig. 2J and figs. S8E and S13, A and B), as expected (*12*). In mESC monochromosomal hybrids, molecules mapping to the telomeric ends of human chromosomes 4 and 21 increased to a median telomere length of 99 and 108 kb in mESC Hchr4 (4p and 4q, respectively) and 57 kb in mESC Hchr21 (21q), with most molecules measuring between 30 and 120 kb (Fig. 2J and fig. S13, A and B). For human chromosome 20 in mESC Hchr20 (CB20F) (20p and 20q), median telomere length similarly increased to 68 and 60 kb (20p and 20q, respectively) (figs. S8E and S13C). The telomere molecule lengths for the human chromosome arms in mESCs were comparable to the telomere molecule lengths of endogenous mouse chromosomes (~100 kb) in the same clones (Fig. 2J and figs. S8E and S13D) and to mouse telomere lengths reported in the literature (*13*). This indicated that after transfer of human chromosomes to mESCs, their telomeres were actively lengthened to match the setpoint for mouse telomere length and were then maintained at this length.

Manipulation of human chromosomes in assembly cells

We set out to replace a region of Hchr20 (35.69 to 35.70 Mb) with synthetic DNA in which 23 wild-type codons (within the *ROMO1* and *NFS1* loci) were replaced with their synonyms (fig. S14A). We first integrated a landing pad comprising a cassette encoding blue fluorescent protein (BFP) and HygR into Hchr20 (fig. S14B) harbored within an assembly cell. We then electroporated a 35-kb bacterial artificial chromosome (BAC) carrying a 10-kb synthetic DNA payload with putatively silent watermarks and a selection cassette encoding mCherry and PuroR, and then cut the human chromosome using CRISPR-guided Cas9 to induce HR-mediated replacement of the landing pad with the (mostly) homologous synthetic DNA carried in the BAC (fig. S14C). Successful integration of the synthetic DNA in Hchr20 in the puromycin-resistant clones was confirmed with polymerase chain reaction genotyping (correct for 7 of 24 clones). For one correctly genotyped clone, we further confirmed successful marker swap using flow cytometry (fig. S14D) and the correct sequence using ONT (fig. S14E). These experiments demonstrated that the sequence of human chromosomes can be precisely manipulated in mESC assembly cells.

Transfer of human chromosomes from mESC monochromosomal hybrids to human cells

Next, we aimed to generate chromosome-specific aneuploidies in human cells through the transfer of human chromosomes from their mESC monochromosomal hybrid hosts to human cells. We were not able to deliver human chromosomes from mESC monochromosomal hybrids to RPE1 cells by PEI transfection. We therefore devised rapid microcell–mediated chromosome transfer (R-MMCT) to transfer chromosomes from mESCs to RPE1 cells. Unlike standard MMCT, which requires 2 to 4 days of colcemid-induced mitotic arrest, often causes micronuclei and chromosome fragmentation and reduced clone viability, and can only be used to transfer chromosomes from the very limited number of cell types that can tolerate hyperploidization (A9 and CHO) (*14*–*18*), R-MMCT minimizes the length of colcemid treatment to effectively arrest cells in mitosis (fig. S15). We used these mitotic cells to generate microcells (*19*), which were filtered for size and fused to RPE1 cells with inactivated Sendai virus [hemagglutinating virus of Japan envelope (HVJ-E)] particles (*9*, *20*). Recipient RPE1 cells were selected, with G418, for the presence of the transferred chromosome (Fig. 3A), achieving a transfer efficiency of ~10^{-6}.

We obtained 107, 51, and 42 RPE1 clones with the correct phenotype from separate R-MMCT experiments using mESC Hchr21 (CT2-1), Hchr4 (CL3), and Hchr20 (CB20F) as donors, respectively. From these clones, we selected 110 clones (30 for Hchr21, 49 for Hchr4, and 31 for Hchr20) for further characterization (fig. S16, table S2, and supplementary text). We investigated chromosome copy number using low-coverage WGS and flow cytometry–based karyotyping and chromosome stability using sfGFP measurements (figs. S17 and S18 and supplementary text).

We performed more detailed characterization of two trisomies, Hchr4 (2A8) and Hchr21 (7M5-1-2), and two tetrasomies, Hchr4 (OB1) and Hchr20 (2A2), for which low-coverage WGS, sfGFP stability, and flow karyotyping were consistent with the presence of an intact and stable aneuploidy (Fig. 3 and fig. S19). G-banding karyotypes of all human chromosomes from these four clones demonstrated the expected copy number increase, resulting from the transferred chromosome (Fig. 3, B and C, and fig. S19, A and B). We did also not detect any karyotypic alterations with respect to RPE1 (fig. S2) in the other chromosomes (Fig. 3, B and C, and fig. S19, A and B). We next performed high-coverage Illumina sequencing, ONT, and Bionano OGM on these clones and control RPE1 clones (Fig. 3, D to I; fig. S19, C to H; and supplementary text). Overall, our data suggested that it is possible to transfer intact human

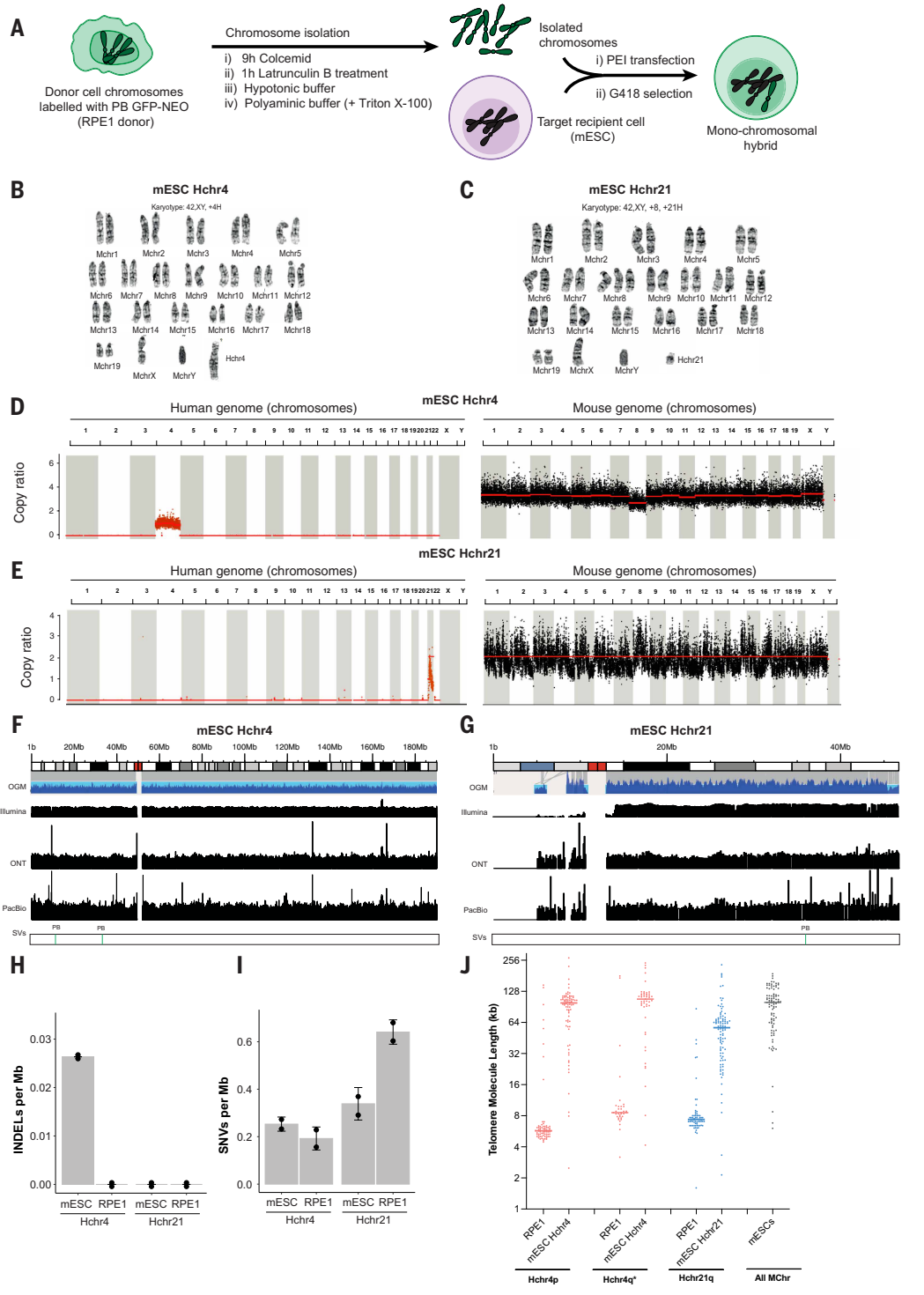

Fig. 2. Human chromosomes can be transfected into mESCs, where they are stably maintained with minimal damage and mouse-length telomeres. (**A**) Schematic of chromosome isolation from RPE1 cells and transfection into mESCs to generate monochromosomal hybrid cells. (**B** and **C**) Giemsa-stained karyotype (G-banding) representative of 20 metaphase spreads of mESCs harboring Hchr4 (clone CL3) (B) and of mESCs harboring Hchr21 (clone CT2-1) (C). (**D** and **E**) CNV analysis of high-coverage Illumina sequencing (NGS) reads for hybrid mESCs with Hchr4 (D) and Hchr21 (E) aligned against a hybrid human-mouse reference genome (bin size, 1 kb). (**F** and **G**) Deep characterization of the transferred Hchr4 (F) and Hchr21 (G) by OGM, high-coverage Illumina, and ONT sequencing. The traces represent the contigs assembled from OGM (blue), and Illumina, ONT, and PacBio coverage. Note that the p arm of Hchr21 cannot be assembled because of its highly repetitive sequence. SVs, including *PiggyBac* insertions (PB), on the transferred chromosome are shown. (**H**) Quantification of INDELs (Illumina) in Hchr4 and Hchr21 compared with two control RPE1 clones. Data are presented as the number of INDELS/Mb with their SDs. (**I**) Quantification of SNVs (Illumina) in Hchr4 and Hchr21 compared with two control RPE1 clones. Data are presented as the number of SNVs/Mb with their SDs. (**J**) Median telomere molecule length (horizontal line) for transfected Hchr4 and Hchr21 (q arm) in monochromosomal hybrid mESCs (Hchr4 clone CL3 and Hchr21 clone CT2-1) compared with the same arms in wild-type RPE1 cells (clone F8) (see the materials and methods). Median telomere molecule length for a subset of representative mouse chromosomes is shown for reference.

chromosomes from mESC monochromosomal hybrid assembly cells to human cells using R-MMCT without retaining mouse DNA (fig. S20) and with minimal DNA damage and mutagenesis, as judged by measurements of SNVs, INDELs, and SVs (Fig. 3H, figs. S19G and S21, and table S3).

After clones were expanded to at least 10^7 cells and then kept in culture for at least six additional passages, we estimated the length of the telomeres of Hchr4p and Hchr4q in the Hchr4 tetrasomy OB1 and Hchr4 trisomy 2A8, of Hchr20p and Hchr20q in Hchr20 tetrasomy 2A2, and of Hchr21q in Hchr21 trisomy 7M5-1-2 from the OGM data. For Hchr4, Hchr20, and Hchr21, most molecules mapping to the telomeres were of similar length to those from wild-type RPE1 cells. However, a fraction of telomeric molecules for Hchr21q in Hchr21 trisomy (7M5-1-2), Hchr4p and Hchr4q in Hchr4 trisomy (2A8), and tetrasomy (OB1) and Hchr20p and Hchr20q in tetrasomy (2A2) were substantially longer (15 to 150 kb) than the telomere molecules in the control RPE1 cells (5 to 10 kb) (Fig. 3I and figs. S19H and S22). This observation suggested that the telomeres of the transferred human chromosomes were generally shorter than when harbored in mESCs and may approach the length of human telomeres with further passaging. The rate of telomere

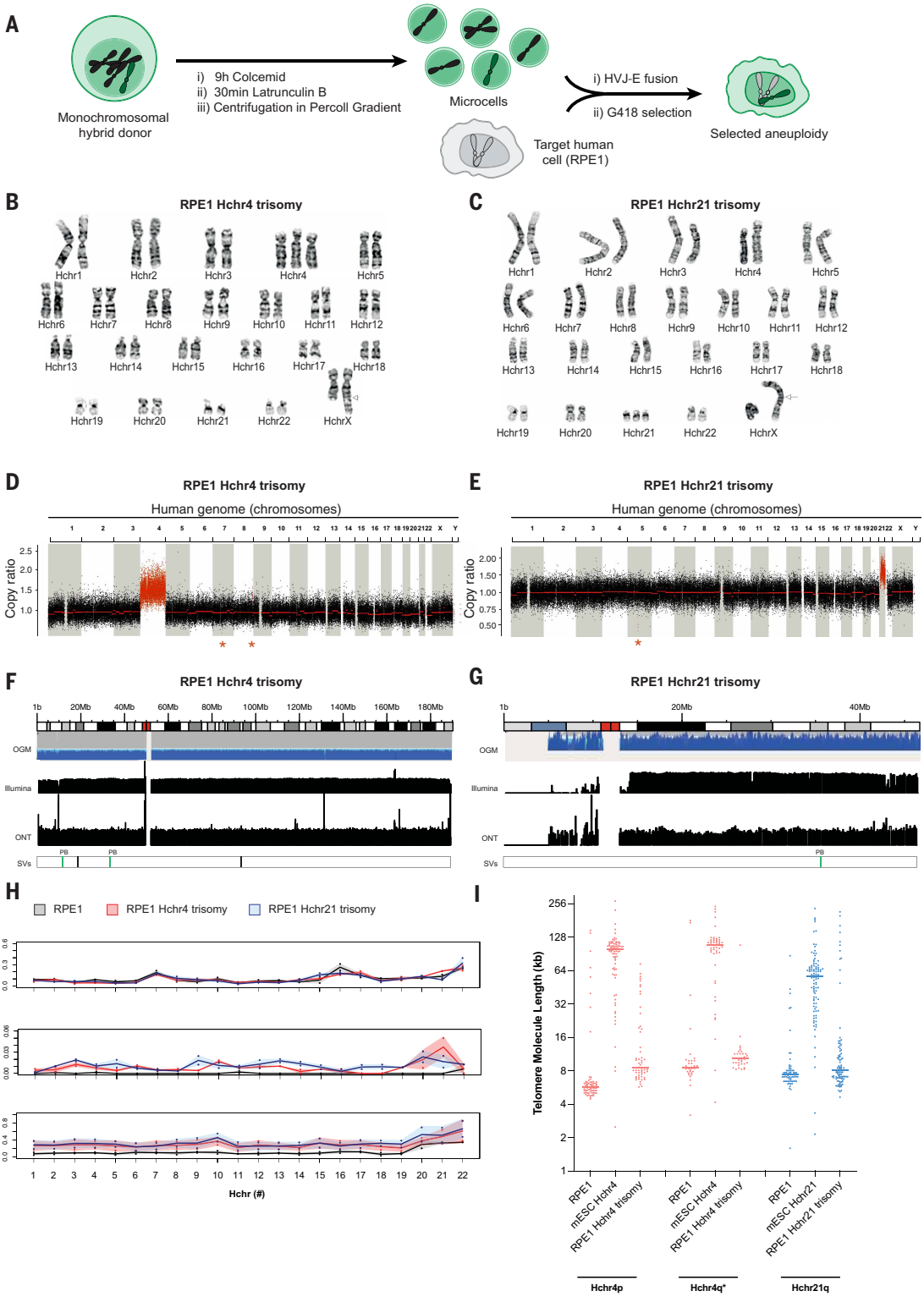

Fig. 3. R-MMCT of human chromosomes from monochromosomal hybrid mESCs to human RPE1 cells to generate defined aneuploidies with minimal damage. (**A**) Schematic of human chromosome transfer from monochromosomal hybrid mESCs to RPE1 cells by R-MMCT to generate specific chromosome aneuploidies. (**B** and **C**) Giemsa-stained karyotype (G-banding) representative of 20 metaphase spreads of Hchr4 RPE1 trisomy (clone 2A8) (B) and Hchr21 RPE1 trisomy (clone 7M5-1-2) (C). (**D** and **E**) CNV analysis of high-coverage Illumina sequencing (NGS) reads for Hchr4 (D) and Hchr21 (E) RPE1 trisomies aligned against a hybrid human-mouse reference genome (bin size, 1 kb). (**F** and **G**) Deep characterization of Hchr4 (F) and Hchr21 (G) in their corresponding RPE1 trisomies by OGM, high-coverage Illumina, and ONT sequencing. The traces represent the contigs assembled from OGM (blue), Illumina, and ONT coverage. SVs, including *PiggyBac* insertions (PB), on the transferred chromosome are shown. Note that the p arm of Hchr21 cannot be assembled because of its highly repetitive sequence. (**H**) Genome-wide analysis of SVs (>40 bp, ONT), SNVs, and INDELs (Illumina) in the Hchr4 and Hchr21 RPE1 trisomies compared with two control RPE1 clones. Data are presented as means with SDs. (**I**) Median telomere molecule length (horizontal line) for Hchr4 and Hchr21 (21q) in their corresponding RPE1 trisomies and in their monochromosomal hybrid mESCs and median telomere molecule length for these chromosomes in RPE1 cells (clone F8) (same data as in Fig. 2J).

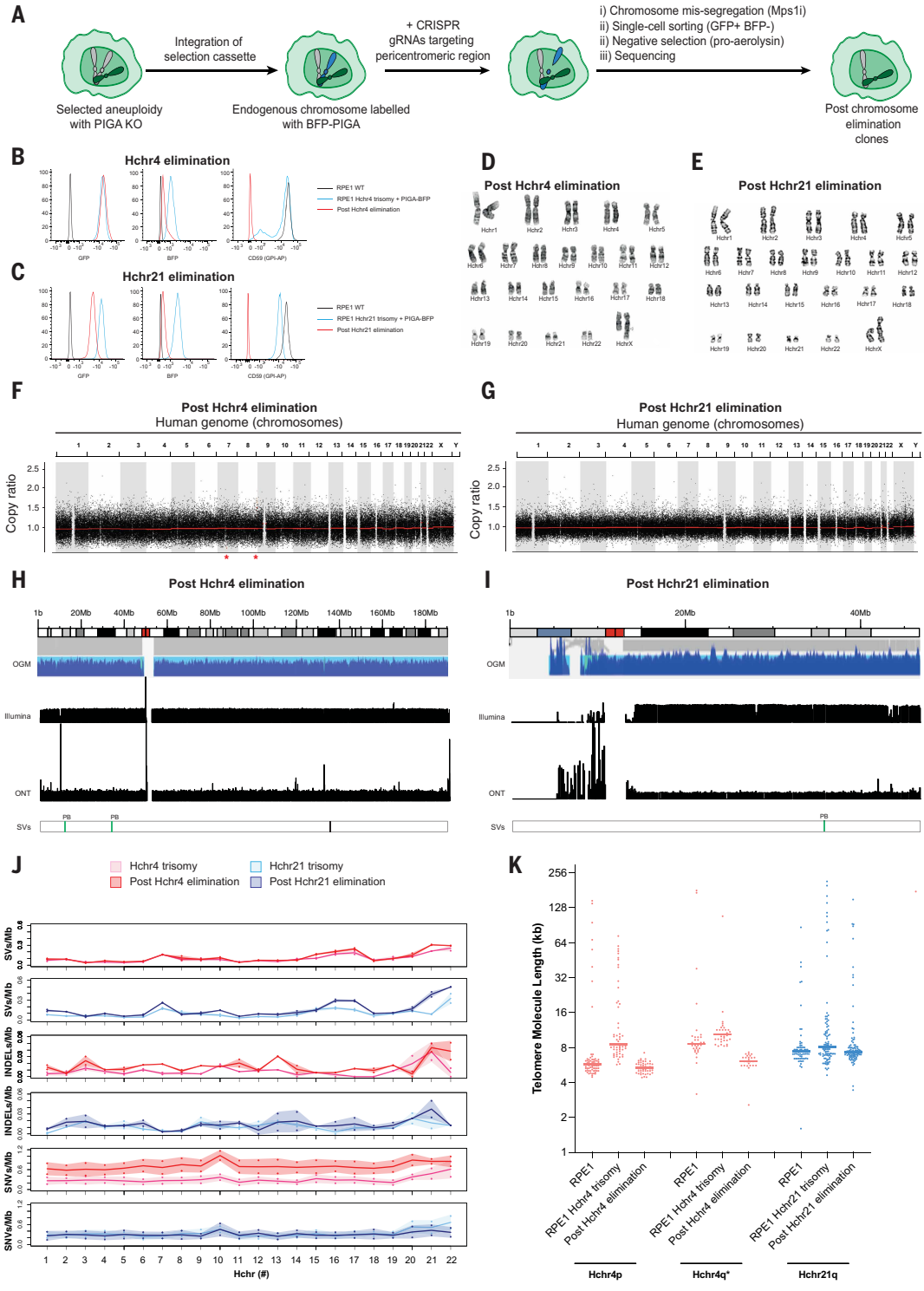

Fig. 4. Targeted removal of aneuploid endogenous chromosomes from human (RPE1) trisomies. (**A**) Schematic of the targeted removal of aneuploid chromosomes from RPE-1 cells. (**B** and **C**) Elimination of the BFP-*PIGA*–marked endogenous chromosome and maintenance of the transferred Hchr4 (clone 35) (B) or Hchr21 (clone 2) (C) was confirmed by flow cytometry. *PIGA* expression was analyzed using an anti-CD59 antibody. The lines show wild-type RPE1 cells for reference (black), the BFP-*PIGA*-marked trisomy (gray), and the eliminated clone. (**D** and **E**) Giemsa-stained karyotype (G-banding) representative of 20 metaphase spreads, all of which show a copy number of two for Hchr4 (clone 35) (D) and similarly for Hchr21 (clone 2) (E). (**F** and **G**) CNV analysis of high-coverage Illumina sequencing (NGS) reads for RPE1 Hchr4 elimination (F) and RPE1 Hchr21 elimination (G) aligned against a hybrid human-mouse reference genome (bin size, 1 kb). (**H** and **I**) Deep characterization of Hchr4 (H) and Hchr21 (I) after chromosome elimination by OGM, high-coverage Illumina, and ONT sequencing. The traces represent the contigs assembled by OGM (blue), Illumina, and ONT coverages. SVs, including *PiggyBac* insertions (PB), in this chromosome are shown. Note that the sequence for the p arm of Hchr21 cannot be assembled because of its highly repetitive sequence. (**J**) Genome-wide analysis of SVs (>40 bp, ONT), SNVs, and INDELs (Illumina) for postelimination clones of Hchr4 and Hchr21 and their corresponding RPE1 trisomies compared with two control RPE1 clones. Data are presented as means with SDs. (**K**) Median telomere molecule length for Hchr4 and Hchr21 in postelimination clones of Hchr4 and Hchr21 and in the corresponding trisomies (same data as in Fig. 3I) and median telomere molecule length for these chromosomes in RPE1 cells (clone F8).

shortening after chromosome transfer appeared to be substantially higher than could be explained by normal telomere attrition during replication (*21*); this suggested that the shortening we observed occurs through a different, and currently unknown, mechanism by which the new host (human) rapidly adjusts telomere length of the transferred human chromosome back to that of its endogenous chromosomes (*22*).

Elimination of endogenous human chromosomes from aneuploid clones

To eliminate an endogenous human chromosome (Fig. 4A), 4 or 21, from our previously generated RPE1 trisomies, we created RPE1 *PIGA* knockouts (fig. S23A and table S4) and introduced a counterselectable *PIGA* marker (*23*), along with a BFP marker, into one of the aneuploid endogenous chromosomes (fig. S23B, table S4, and supplementary text).

We then targeted the pericentromeric sequence of the aneuploid chromosome for CRISPR-mediated cleavage (table S4); transiently inhibited the mitotic checkpoint; sorted for sfGFP-positive, BFP-negative cells to enrich for cells that had maintained the transferred chromosome and lost the selection cassette; and then selected with proaerolysin to identify clones in which we had achieved successful chromosome elimination (Fig. 4, A to C; fig. S24; and supplementary text). A subset of the resultant proaerolysin-resistant clones were analyzed by Illumina short-read WGS (fig. S25). Copy number analysis of these clones confirmed successful elimination of Hchr4 and Hchr21 from their respective trisomic clones (2A8 and 7M5-1-2) with a success rate of >95% (fig. S25). We did not detect any off-target chromosome gains or losses (fig. S25).

Next, we selected clones elCL18 and elCL35, resulting from elimination of an endogenous Hchr4 from the trisomic clone 2A8, and clones elCL1 and elCL2, resulting from the elimination of an endogenous Hchr21 from the trisomic clone 7M5-1-2, for further characterization. We performed G-banding analysis; flow karyotyping; and high-coverage Illumina WGS, ONT, and OGM analysis (Fig. 4, D to K; figs. S26 and S27; and supplementary text) and specifically checked for CRISPR off-targets (tables S5 and S6 and supplementary text). These experiments demonstrated that these clones were diploid and the transferred chromosome intact (Fig. 4, D to I, and fig. S26), with the exception of a pericentromeric copy number change in one of the clones (fig. S27, C and D). We also found that the levels of SVs, INDELs, and SNVs in these postelimination clones were essentially comparable to the levels in the aneuploidies from which they were directly derived (Fig. 4J, fig. S28, table S3, and supplementary text).

The median telomere molecule lengths for Hchr4p and Hchr4q after elimination (elCL35) were 5.32 and 6.07 kb, respectively, and resembled the median telomere molecule length of the wild-type RPE1 control (5.72 and 8.60 kb for Hchr4p and Hchr4q, respectively) (Fig. 4K and fig. S29). Similarly, for Hchr21q, we found a median telomere molecule length of 7.34 kb, which was indistinguishable from that found in the wild-type RPE1 (7.37 kb) (Fig. 4K and fig. S29). Therefore, our data confirmed that telomere length returns to that of wild-type RPE1 cells after chromosome elimination and passaging.

Discussion

Here, we have provided a high-fidelity workflow for moving human chromosomes into mESC assembly cells, where they can be operated on, and returning them into human cells with regeneration of the normal karyotype. Chromosome transfection and R-MMCT proceeded with comparable high fidelity, and comparable efficiency, for the chromosome transfers tested; the preferred method of chromosome transfer will be a function of the properties of the donor and recipient cells. The intermediate aneuploidies provide a resource for studying the consequences of defined chromosome copy number changes without the confounding effects of cancer mutations. Advances in building and delivering episomes containing megabases of synthetic DNA and in replacing large chromosomal regions in mESCs (*24*–*28*) may be combined with the approaches reported herein to accelerate the synthesis of human genomes.

REFERENCES AND NOTES

1. D. G. Gibson *et al.*, *Science* **319**, 1215–1220 (2008).
2. J. Fredens *et al.*, *Nature* **569**, 514–518 (2019).
3. S. M. Richardson *et al.*, *Science* **355**, 1040–1044 (2017).
4. D. Schindler *et al.*, *Cell* **186**, 5237–5253.e22 (2023).
5. A. G. Bodnar *et al.*, *Science* **279**, 349–352 (1998).
6. E. Volpe *et al.*, *Nat. Commun.* **16**, 7751 (2025)
7. S. Ding *et al.*, *Cell* **122**, 473–483 (2005).
8. S. J. Elsässer, R. J. Ernst, O. S. Walker, J. W. Chin, *Nat. Methods* **13**, 158–164 (2016).
9. M. Liskovykh, N. C. Lee, V. Larionov, N. Kouprina, *Mol. Ther. Methods Clin. Dev.* **3**, 16043 (2016).
10. B. L. Ng, N. P. Carter, *Cytometry A* **69**, 1028–1036 (2006).
11. E. Young *et al.*, *Nucleic Acids Res.* **45**, e73 (2017).
12. M. A. Blasco, *Nat. Rev. Genet.* **6**, 611–622 (2005).
13. E. Varela, R. P. Schneider, S. Ortega, M. A. Blasco, *Proc. Natl. Acad. Sci. U.S.A.* **108**, 15207–15212 (2011).
14. M. Paulis *et al.*, *Mol. Ther. Methods Clin. Dev.* **17**, 369–377 (2020).
15. T. Ege, N. R. Ringertz, *Exp. Cell Res.* **87**, 378–382 (1974).
16. R. E. Fournier, F. H. Ruddle, *Proc. Natl. Acad. Sci. U.S.A.* **74**, 319–323 (1977).
17. T. Suzuki, Y. Kazuki, M. Oshimura, T. Hara, *PLOS ONE* **11**, e0157187 (2016).
18. N. Uno *et al.*, *Sci. Rep.* **12**, 3009 (2022).
19. E. Stubblefield, M. Pershouse, *Somat. Cell Mol. Genet.* **18**, 485–491 (1992).
20. S. Yamaguchi, X. Ren, M. Katoh, *Chromosome Sci.* **9**, 65–73 (2006).
21. C. B. Harley, A. B. Futcher, C. W. Greider, *Nature* **345**, 458–460 (1990).
22. A. Weuts *et al.*, *Nucleic Acids Res.* **40**, 11477–11489 (2012).
23. D. Li *et al.*, *Nucleic Acids Res.* **49**, 2642–2654 (2021).
24. L. Li, T. Blankenstein, *Nat. Protoc.* **8**, 1567–1582 (2013).
25. E. C. Lee *et al.*, *Nat. Biotechnol.* **32**, 356–363 (2014).
26. H. A. Wallace *et al.*, *Cell* **128**, 197–209 (2007).
27. W. Zhang *et al.*, *Nature* **623**, 423–431 (2023).
28. R. Brosh *et al.*, *Proc. Natl. Acad. Sci. U.S.A.* **118**, e2023952118 (2021).

ACKNOWLEDGMENTS

We thank the staff of the Flow Cytometry Facility at the MRC Laboratory of Molecular Biology, including M. Daly, P. A. Penttilä, Y. Li, and F. Zhang; G. van der Goot (EPFL, Lausanne) for supplying purified proaerolysin; scientists and staff at Bionano Genomics and Source Bioscience, especially L. Laws, E. Shaffu, E. Mularczyk, and H. Horn; the Wellcome Sanger Institute, CASM program support, and the DNA pipeline and long-read teams for ONT and OGM analysis, especially K. Oliver, I. Bronner, M. Dignam, G. Ping, and M. Smith; and the UCL Long Read Sequencing service, especially J. Lee, for Bionano OGM and PacBio sequencing. JM8.F6 mouse embryonic stem cells (mESCs) were obtained from the Wellcome Sanger Institute (Hinxton, UK). **Funding:** This work was supported by the UK Medical Research Council (MRC grants MC_U105181009 and MC_UP_A024_1008 to J.W.C. and grant MC_U105178808 to J.E.S.) and the Wellcome Trust (discretionary award 221267/Z/20/Z to J.W.C. and J.E.S.). S.G. was supported by the Boehringer Ingelheim Fonds and the Cambridge Commonwealth, European and International Trust. G.P. was partially supported by a Marie Skłodowska-Curie European Postdoctoral Fellowship (897663). J.W.C. and J.E.S. thank the Wellcome Sanger Institute for support through the associate faculty program. **Author contributions:** Conceptualization: G.P., S.G., L.V.B., J.E.S., J.W.C.; Formal analysis: P.M., K.C.L., S.G.; Funding acquisition: J.W.C., J.E.S.; Investigation: G.P., S.G., L.V.B., J.B.; Methodology: G.P., S.G., L.V.B., P.M., K.C.L.; Supervision: J.E.S., J.W.C.; Writing – original draft: G.P., S.G., L.V.B., J.E.S., J.W.C.; Writing – review & editing: G.P., S.G., L.V.B., P.M., K.C.L., J.E.S., J.W.C. **Competing interests:** J.W.C. is founder of Constructive Bio and K.C.L. is a consultant for Constructive Bio. G.P. is founder of Alia Therapeutics. The remaining authors declare no competing interests. **Data and materials availability:** Data for the present paper can be found in the Sequence Read Archive of the National Center for Biotechnology Information (https://www.ncbi.nlm.nih.gov/sra) under bioproject number PRJNA1201099. The scripts used for data analysis can be found at 10.5281/zenodo.17642095. The authors agree to provide any materials and cell lines generated in this study upon request. This research was funded in whole or in part by the UK Medical Research Council (grants MC_U105181009, MC_UP_A024_1008, and MC_U105178808) and by Wellcome (discretionary award 221267/Z/20/Z), both cOAlition S organizations. The author will make the Author Accepted Manuscript (AAM) version available under a CC BY public copyright license.

SUPPLEMENTARY MATERIALS

science.org/doi/10.1126/science.adv9797
Materials and Methods; Supplementary Text; Figs. S1 to S29; Tables S1 to S6; References (*29*–*81*); MDAR Reproducibility Checklist

Submitted 14 January 2025; resubmitted 20 June 2025; accepted 9 October 2025
10.1126/science.adv9797